INTERNATIONAL JOURNAL FOR NUMERICAL METHODS IN FLUIDS
Int. J. Numer. Meth. Fluids 2001; **36**: 265–285 (DOI: 10.1002/fld.131)

Finite element simulation of fully non-linear interaction between vertical cylinders and steep waves. Part 1: Methodology and numerical procedure

Q. W. Ma[a,*], G. X. Wu[a] and R. Eatock Taylor[b]

[a] *Department of Mechanical Engineering, University College London, Torrington Place, London, U.K.*
[b] *Department of Engineering Science, University of Oxford, Parks Road, Oxford, U.K.*

SUMMARY

A methodology for computing three-dimensional interaction between waves and fixed bodies is developed based on a fully non-linear potential flow theory. The associated boundary value problem is solved using a finite element method (FEM). A recovery technique has been implemented to improve the FEM solution. The velocity is calculated by a numerical differentiation technique. The corresponding algebraic equations are solved by the conjugate gradient method with a symmetric successive overrelaxation (SSOR) preconditioner. The radiation condition at a truncated boundary is imposed based on the combination of a damping zone and the Sommerfeld condition. This paper (Part 1) focuses on the technical procedure, while Part 2 [Finite element simulation of fully non-linear interaction between vertical cylinders and steep waves. Part 2. Numerical results and validation. *International Journal for Numerical Methods in Fluids* 2001] gives detailed numerical results, including validation, for the cases of steep waves interacting with one or two vertical cylinders. Copyright © 2001 John Wiley & Sons, Ltd.

KEY WORDS: boundary value problem; finite element method; non-linear potential flow; waves

1. INTRODUCTION

The fully non-linear body–wave interaction problem is usually solved based on the potential flow theory, through a time step marching procedure developed from the work of Longuet-Higgins and Cokelet [1]. It assumes that the wave profile and the position of the structure are known at a particular instant. The problem can then be solved by numerical techniques. The Bernoulli equation enables us to find the force on the structure. If the structure is not fixed, Newton's law will give the new acceleration. The acceleration then gives a new velocity, which further gives the new position of the structure. Similarly, the velocity obtained on the free

* Correspondence to: Department of Mechanical Engineering, University College London, Torrington Place, London WC1E 7JE, U.K.

Received June 1999
Revised November 1999

surface will give a new free surface profile. All these will enable the problem to be solved at the next time step. The procedure can be repeated in principle for any given period of time.

The solution of the velocity potential at each time step is found by solving a mixed boundary value problem, which forms a key part of the fully non-linear analysis. This boundary value problem has been solved in many publications by a boundary element method (BEM). The BEM has provided a very powerful tool for solving linear and second-order body–wave interaction in the frequency domain. A distinct advantage of the method is that a Green function, satisfying both governing equations and all the boundary conditions except that on the body surface, can be found. As a result, in numerical analysis it is necessary to discretize only the body surface where unknown sources are distributed. In the second-order problem, the discretization of the free surface may also be needed, but this is only for the purpose of numerical integration of some known functions over the surface. When the BEM is adopted in the time domain problem, a Rankine source Green function is usually used. This Green function is very simple to evaluate, but the distribution of sources on all the boundaries of the fluid domain is necessary rather than only on the body surface. Many applications, such as in References [2–5], have been made using this formulation to analyse the second-order wave diffraction and radiation problem in the time domain.

The application of the BEM to the fully non-linear problem was initiated by Longuet-Higgins and Cokelet [1] and followed by Faltinsen [6], Vinje and Brevig [7] and Lin *et al*. [8]. More recent publications include References [9–13]. A modified version of the BEM was proposed by Cao *et al*. [14] and Beck *et al*. [15], in which the sources are distributed on an artificial surface outside the fluid domain, but the conditions are still imposed on the physical boundaries of the fluid domain. This method is referred to as the 'desingularized' BEM. Unlike the conventional BEM, the Green function in the desingularized BEM does not have any singular points in the fluid domain and on its boundaries.

Although many successful simulations of the fully non-linear problem have been achieved through the BEM, its unique advantage associated with linear and second-order problems no longer exists here. When the unknown sources are distributed over the entire boundary of the fluid domain, it usually leads to a dramatic increase of the number of influence coefficients because of the fully populated matrix, which has to be assembled and solved at each time step. As a result, massive computing and storage requirements are needed for many practical cases. Indeed, Celebi *et al*. [13] reported that even for a single circular cylinder, the simulation over 20 wave periods took about 20 h of CPU on a CRAY J90. Some efforts have been made to reduce the CPU time and memory requirement by using the domain decomposition technique [16] but success has been reported only for some special two-dimensional problems. The effectiveness of this technique for more general cases, especially for the three-dimensional problem, is still not clear.

By contrast, the finite element method (FEM) has some different features. Unlike the BEM, the FEM requires the entire fluid domain to be discretized. Therefore, the number of nodes and unknowns in the FEM is much larger than in the BEM. However, in the FEM a node is influenced only by those nodes directly linked to it. This means that in each line of the coefficient matrix, there are only a few non-zero terms. Therefore, the number of non-zero entries in the FEM will be much less than in the BEM for this kind of problem, which implies that much less storage and CPU may be required. In addition, there is no need to deal with

the singularity associated with the Rankine source, and the coefficient evaluation in the FEM is very simple. These further distinguish the FEM from the BEM. Wu and Eatock Taylor [17,18] have applied the FEM to cases of fully non-linear two-dimensional interaction between waves and bodies. They investigated different discretized formulations of the problem by considering the velocity potential as unknown (FEM) or the potential as well as two velocity components as unknown (hybrid FEM). It was suggested that the hybrid FEM did not seem to be superior in terms of accuracy, despite considerably more memory and CPU being required. The algebraic equations in their work were solved using the Choleski factorization method. Remeshing was performed at each time step following the change of the fluid domain. They provided various results, including waves generated by a piston wave maker, starting suddenly from rest or undergoing harmonic oscillations; standing waves in a container; and forced oscillation of a cylinder in open water. Reflected waves were avoided by truncating the fluid domain at a sufficiently large distance from the body and stopping the calculation before the reflection became clearly visible. Later, Cai *et al.* [19] developed a finite element formulation for fully non-linear water waves based on a time-dependent mapping of the fluid domain onto a fixed computational rectangle. This technique can avoid the need for remeshing the imaginary computational domain during the wave evolution. Recently, however, Westhuis and Andonowati [20] showed that this mapping technique may not give results as good as those obtained by the method in which the fluid domain is directly discretized.

Wu and Eatock Taylor [18] also made a comparison between the FEM and the BEM for a two-dimensional wave radiation problem. The results suggested that the FEM was more efficient in terms of storage requirement and solution time than the equivalent BEM. Even when the decomposition technique by Wang *et al.* [16] is applied, the number of non-zero coefficients in the BEM may still be no less than the FEM [21]. Westhuis and Andonowati [20] also made a similar comparison more recently. Their results confirmed the conclusion of Wu and Eatock Taylor [18].

In the present paper we apply the FEM to analyse the fully non-linear three-dimensional interaction between waves and fixed bodies. An iterative method with a preconditioner is used to solve the algebraic equations. A postprocessor based on the recovery technique is adopted in order to improve the accuracy of the finite element solution without increasing the number of elements. A radiation condition is imposed, which is to minimize the effect of the reflection of waves from the truncated boundary of the fluid domain. In addition, procedures for evaluating the fluid velocities and for calculating the forces on bodies are discussed. The overall methodology is applied in Part 2 of this series [22] to various cases associated with the interaction between steep waves and vertical cylinders in a tank. It appears that such an application of the FEM to the interactions between fully non-linear waves and single or multiple bodies has not previously been published.

2. MATHEMATICAL FORMULATION

The wave is generated in the tank by a piston-like wave maker. A sketch of the problem with the definition of some dimensions is shown in Figure 1. A Cartesian co-ordinate system is used with the oxy plane on the mean free surface and with the z-axis being positive upwards. The

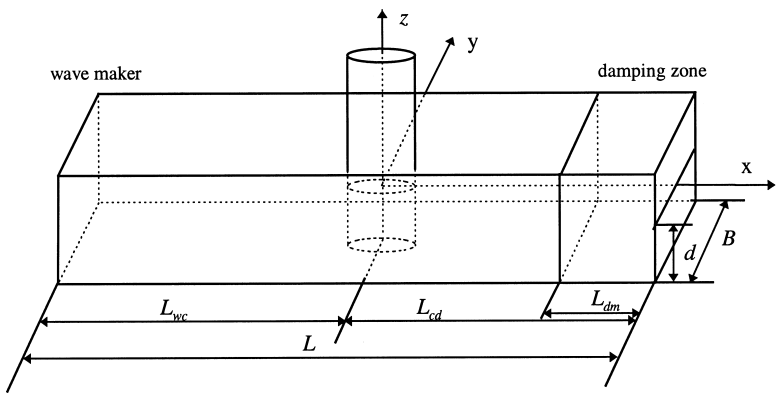

Figure 1. Sketch of the problem.

wave maker is mounted at the left-hand end (on the negative side of the x-axis) and a damping zone with a Sommerfeld condition (see Section 2.2) is applied at the other end of the tank.

2.1. Governing equation and boundary conditions of fluid motion

The viscosity, surface tension and compressibility are neglected. The fluid flow is then irrotational so that a velocity potential, $\phi(x, y, z, t)$, exists and the fluid velocity, $\boldsymbol{u}$, is given by its gradient, or $\boldsymbol{u} = \nabla\phi$. The velocity potential satisfies the Laplace equation in the fluid domain

$$\nabla^2\phi = 0 \tag{1}$$

On the free surface $z = \zeta(x, y, t)$, the kinematic and dynamic conditions can be written in the following Lagrangian form:

$$\frac{\mathrm{D}x}{\mathrm{D}t} = \frac{\partial\phi}{\partial x}, \qquad \frac{\mathrm{D}y}{\mathrm{D}t} = \frac{\partial\phi}{\partial y}, \qquad \frac{\mathrm{D}z}{\mathrm{D}t} = \frac{\partial\phi}{\partial z} \tag{2}$$

$$\frac{\mathrm{D}\phi}{\mathrm{D}t} - \frac{1}{2}|\nabla\phi|^2 + gz = 0 \tag{3}$$

where g is the acceleration due to the gravity. The atmospheric pressure on the free surface has been taken as zero in Equation (3). The condition on the wave maker can be expressed as

$$\frac{\partial\phi}{\partial x} = U(t) \tag{4}$$

where $U(t)$ is the velocity of the wave maker and the condition is imposed at its instantaneous position. On the rigid surfaces, including the cylinder surface, side-walls and bottom, the condition is

$$\frac{\partial \phi}{\partial \boldsymbol{n}} = 0 \tag{5}$$

where $\boldsymbol{n}$ is the normal vector of the surface pointing out of the fluid domain.

2.2. Wave absorption

In addition to the above conditions, a proper condition should be specified at the downstream end (far end) in order to eliminate reflections as much as possible. Several techniques have been suggested in various publications. These include a periodic boundary condition [1], a Sommerfeld condition [23], an absorbing condition based on different equations [24], matching with the far field linear solution [8], an active wave absorber [25,26], and a damping zone [15,16,27]. In addition, there are schemes based on some combination of the above techniques. Arai *et al.* [28] combined the velocity reduction method with the Sommerfeld condition. Contento and Casole [29] coupled the normal damping zone method with the Sommerfeld condition. Clement [30] employed the combination of an active wave absorber and the damping zone method.

Although the results have demonstrated that the above techniques can absorb the wave quite effectively in many cases, none of these can completely remove the reflection of fully non-linear waves. In our application, the scheme is based on a combination of the damping zone and the Sommerfeld condition. An empirical formula for the damping coefficient used in this scheme will be given, which is obtained from the extensive numerical tests and curve fitting.

The Sommerfeld condition gives

$$\frac{\partial \phi}{\partial t} + c \frac{\partial \phi}{\partial \boldsymbol{n}} = 0 \tag{6}$$

where $\boldsymbol{n}$ is the normal vector out of the truncated boundary. A difficulty in implementing this condition is how to evaluate the parameter c, which is the phase velocity of a linear harmonic wave. Its physical meaning cannot exactly be identified when the equation is applied to fully non-linear waves. In some reported applications, the parameter at each time step is simply estimated by the numerical values of $\partial\phi/\partial t$ and $\partial\phi/\partial n$ at previous steps, see, for example, References [29,31,32]. However, in this approach large errors are not easily avoided, particularly when the crest or trough of the velocity potential passes the truncated boundary. Attempts have been made to overcome this difficulty. Contento and Casole [29] used an average value of c found from a number of points near the boundary. The results, however, often oscillate rapidly with time, which may make numerical instability more likely. An alternative is to take c as a constant, particularly when combining the Sommerfeld condition with other techniques. Ohyama [33] used $c/\sqrt{gd} = 1$, which is the phase velocity of the long wave, when he coupled a sponge layer with the Sommerfeld condition. Arai *et al.* [28] took c

as the phase velocity of the linear harmonic wave when they combined the Sommerfeld condition with a velocity reduction technique. Although these constant value techniques are not consistent with the properties of the fully non-linear wave, they are easier than others to implement. In our work, we chose parameter c in the same way as done by Arai *et al*. [28], i.e. for a harmonic wave

$$\frac{c}{\sqrt{gd}} = \sqrt{\frac{\tanh(kd)}{kd}} \tag{7}$$

where d is the depth of water, k is the real root of $\omega^2 = gk \tanh(kd)$ and ω is the wave frequency.

It should be noted that even when the wave is linear and harmonic, Equation (7) is valid only after the generated wave becomes periodic in the tank. Before it reaches the periodic stage, there is a transient zone between the wave front and the truncated boundary. In this zone, the wave is very long, and thus the phase velocity of the wave is different from that in Equation (7) and is close to $c/\sqrt{gd} = 1$. Lee and Leonard [34] have suggested an interpolation between $c/\sqrt{gd} = 1$ and

$$\frac{c}{\sqrt{gd}} = \sqrt{\frac{\tanh(kd)}{kd}}$$

for the transient stage. This interpolation is not implemented in our work because the wave amplitude in this transient zone is relatively small and can be further reduced by the damping zone. The small error in c at this stage, therefore, does not significantly affect the results in which we are interested.

The truncated boundary at the far end can be either fixed or non-fixed. If the boundary is fixed, one has to deal with the situation where the water particles on the boundary move inwards as their velocity components normal to the boundary are not always zero, and thus the boundary becomes detached from the water. In the non-fixed case, the boundary is considered to move with the water particles. However, the boundary in this case may become seriously distorted if each spatial point follows the corresponding water particle. This distortion can lead to numerical difficulties. One way to avoid this is to take the velocity of the boundary motion, U_{rc} (rc denoting radiation condition), as the average of the x-component of the velocity of water particles on the intersection line between the free surface and the boundary. The boundary surface will then move at this velocity in the horizontal direction and will remain vertical at all times.

To implement Equation (6) based on the non-fixed boundary technique, the time derivative of the velocity potential on the truncated boundary is expressed as

$$\frac{\mathrm{d}\phi_{\mathrm{rc}}}{\mathrm{d}t} = \frac{\partial \phi_{\mathrm{rc}}}{\partial t} + U_{\mathrm{rc}} \frac{\partial \phi_{\mathrm{rc}}}{\partial x} + v \frac{\partial \phi_{\mathrm{rc}}}{\partial y} + w \frac{\partial \phi_{\mathrm{rc}}}{\partial z} = \frac{\partial \phi_{\mathrm{rc}}}{\partial t} + U_{\mathrm{rc}} u + v^2 + w^2 \tag{8}$$

where u, v and w are the velocities of fluid particles in the x-, y- and z-directions respectively. Inserting Equation (6) into the above equation yields

$$\frac{\mathrm{d}\phi_{\mathrm{rc}}}{\mathrm{d}t} = (U_{\mathrm{rc}} - c)u + v^2 + w^2$$

In order to be more consistent with the assumption about U_{rc}, u and w here can be replaced by their averages ($\bar{u}$ and $\bar{w}$) along the y-direction at the same depth and v can be assumed to be zero. Then the value of the velocity potential on the truncated boundary is estimated by

$$\begin{cases} \phi_{\mathrm{rc}} = 0 & t \le t_1 \\ \phi_{\mathrm{rc}}|_{t+\Delta t} = \phi_{\mathrm{rc}}|_t + \dfrac{\mathrm{d}\phi_{\mathrm{rc}}}{\mathrm{d}t}\,\Delta t & t > t_1 \end{cases} \tag{9}$$

Here $t_1 = L/[(1+\beta)\sqrt{gd}]$, β is a coefficient that can be taken as 0.2 according to numerical tests. Equation (9) means the velocity potential at the truncated boundary is considered as undisturbed in a period before the wave front reaches it.

It should be noted that there is an inconsistency at the intersection line between the free surface and the vertical boundary at the far end. The non-linear boundary conditions are used on the free surface, but the Sommerfeld condition applied on the truncated vertical surface is linear. The velocity potential is not identical when the points on the intersection line are approached from the two surfaces. This may lead to artificially large velocities and numerical instability. To suppress the problem, a localized interpolation is introduced on the vertical surface in the range $z_{\mathrm{s}} \le z \le z_{\mathrm{f}}$, where z_{f} is the vertical co-ordinate of the intersection line and $z = z_{\mathrm{s}}$ is a line below the free surface on the truncated boundary. In this range, the velocity potential in Equation (9) is replaced by

$$\begin{aligned} \phi_{\mathrm{rc}} = {} & \phi_{\mathrm{s}}\left(1 + 2\frac{z - z_{\mathrm{s}}}{z_{\mathrm{f}} - z_{\mathrm{s}}}\right)\left(\frac{z - z_{\mathrm{f}}}{z_{\mathrm{f}} - z_{\mathrm{s}}}\right)^2 + \phi_{\mathrm{f}}\left(1 - 2\frac{z - z_{\mathrm{f}}}{z_{\mathrm{f}} - z_{\mathrm{s}}}\right)\left(\frac{z - z_{\mathrm{s}}}{z_{\mathrm{f}} - z_{\mathrm{s}}}\right)^2 + w_{\mathrm{s}}(z - z_{\mathrm{s}})\left(\frac{z - z_{\mathrm{f}}}{z_{\mathrm{f}} - z_{\mathrm{s}}}\right)^2 \\ & + w_{\mathrm{f}}(z - z_{\mathrm{f}})\left(\frac{z - z_{\mathrm{s}}}{z_{\mathrm{f}} - z_{\mathrm{s}}}\right)^2 \end{aligned} \tag{10}$$

where $(\phi_{\mathrm{f}}, \phi_{\mathrm{s}})$ and $(w_{\mathrm{f}}, w_{\mathrm{s}})$ are the potentials and vertical velocities at $z = z_{\mathrm{f}}$ and $z = z_{\mathrm{s}}$ respectively. It is easy to show that the velocity potential in the expression satisfies

$$\phi_{\mathrm{rc}} = \phi_{\mathrm{f}}, \qquad \frac{\partial \phi_{\mathrm{rc}}}{\partial z} = w_{\mathrm{f}} \quad \text{for } z = z_{\mathrm{f}}$$

and

$$\phi_{\mathrm{rc}} = \phi_{\mathrm{s}}, \qquad \frac{\partial \phi_{\mathrm{rc}}}{\partial z} = w_{\mathrm{s}} \quad \text{for } z = z_{\mathrm{s}}$$

The length of $(z_{\mathrm{f}} - z_{\mathrm{s}})$ is found to be suitable if it covers three element lengths in the z-direction regardless of the size of elements.

The damping zone is implemented by adding an artificial viscous term in the free surface conditions near the boundary at the far end. The added term removes the energy from the water, and therefore reduces the reflection. Although the dynamic and kinematic conditions on the free surface can both be modified by adding viscous terms, numerical tests in our work have shown that the modification to the kinematic condition sometimes causes sawtooth-like waves in the damping zone. Therefore, the viscous term is added only to the dynamic condition.

After the viscous term has been added, the dynamic free surface condition can be written as

$$\frac{\mathrm{D}\phi}{\mathrm{D}t} = \mathrm{NT} - \nu(x)|\phi|\,\mathrm{sign}(\phi_\mathrm{n}) \tag{11}$$

where NT denotes the normal term in Equation (3), $\nu(x) \geq 0$ is a damping coefficient, $\mathrm{sign}(\phi_\mathrm{n})$ is defined by

$$\mathrm{sign}(\phi_\mathrm{n}) = \begin{cases} -1 & \phi_\mathrm{n} < 0 \\ 0 & \phi_\mathrm{n} = 0 \\ 1 & \phi_\mathrm{n} > 0 \end{cases}$$

and ϕ_n denotes the normal velocity on the free surface. If the wave is not overturning, ϕ_n has the same sign as the vertical velocity, which means that $\mathrm{sign}(\phi_\mathrm{n})$ can be replaced by $\mathrm{sign}(w)$ in the calculation. The added term in Equation (11) ensures that the damping zone always absorbs energy from the fluid, as shown by Cao *et al.* [35].

The choice of the term $\nu(x)$ in Equation (11) is based on empirical considerations. Its magnitude and form play an important role in the performance of the damping zone. If the value is too small, the absorption is too weak, while if it is too big the zone itself acts like a rigid surface. Large reflections occur in both cases, although for different reasons. In addition, $\nu(x)$ has to be smooth enough in the zone and at both of its ends otherwise discontinuities may lead to large gradients of velocity. This not only gives rise to reflections but also may cause numerical instability. In this work, the following form of $\nu(x)$ is adopted:

$$\nu(x) = \begin{cases} \dfrac{1}{2}\nu_0\left(1 - \cos\left(\dfrac{\pi(x - x_\mathrm{d})}{L_\mathrm{dm}}\right)\right) & x \geq x_\mathrm{d} \\ 0 & x < x_\mathrm{d} \end{cases}$$

where ν_0 is the magnitude of the damping coefficient, x_d is the x co-ordinate of the left end of the zone and L_dm is the length of the zone. Evidently, the efficiency of the damping zone depends on both L_dm and ν_0. Here the length is taken as $L_\mathrm{dm} = \min(3\lambda, 3d)$, where $\lambda = 2\pi/k$; an optimal choice of ν_0 will be discussed in Part 2 [22].

It is known from linear theory (see e.g. Reference [36]) that the transient wave generated by a wave maker may be divided into two parts: the progressive wave and the local wave. The progressive wave travels to infinity, whereas the local wave exists only in a region near the

wave maker and decreases with distance from the wave maker at a rate $\exp[-(\pi/2d)(x-x_0)]$ [37], where x_0 is the position of the wave maker. The interaction between the progressive wave and the cylinder is of concern here. To avoid the effect of the local wave, the cylinder is placed sufficiently far from the wave maker. As suggested by Crapper [37], the effects of local waves become negligible when $x - x_0 > 2d$. In the following analysis, the length from the wave maker to the centre of the nearest cylinder, L_{wc}, is taken such that $L_{wc} > R_0 + 3d$, where R_0 is the radius of the cylinder. When the progressive waves reach the cylinder, they will be reflected and transmitted. The reflected waves from the cylinder travel back towards to the wave maker. The interaction between the reflected waves and the wave maker may distort the original progressive waves. Ideally this type of interaction should be removed. In our work, the cylinder is put at a position sufficiently far from the wave maker, and the calculation stops before the distorted waves have travelled back to the cylinder. The maximum time over which the computation is made is estimated as $3L_{wc}/C_g$, where C_g is the group velocity of the wave. Clearly, if a long calculation is required, the value of L_{wc} should be made sufficiently large. This procedure is very similar to the practice in physical experiments, although the influence of the distorted wave may not be avoided completely.

2.3. Force calculation

The force and moment acting on bodies can be evaluated by integrating the pressure over the wetted surface

$$\boldsymbol{F} = -\rho \iint_{S_b} \left(\frac{\partial \phi}{\partial t} + \frac{1}{2} |\nabla \phi|^2 + gz \right) \boldsymbol{n} \, \mathrm{d}S \tag{12}$$

$$\boldsymbol{M} = -\rho \iint_{S_b} \left(\frac{\partial \phi}{\partial t} + \frac{1}{2} |\nabla \phi|^2 + gz \right) \boldsymbol{r} \times \boldsymbol{n} \, \mathrm{d}S \tag{13}$$

where S_b denotes the wetted body surface. As is well known, the evaluation of the $\partial\phi/\partial t$ term is not trivial. Here it is obtained by solving another field equation.

The $\partial\phi/\partial t$ term satisfies the same governing equation in the fluid domain and boundary conditions on the fixed rigid surface as those for the velocity potential. On the free surface, the Bernoulli equation gives

$$\frac{\partial \phi}{\partial t} = -gz - \frac{1}{2} |\nabla \phi|^2 \tag{14}$$

On the wave maker, the condition (see Reference [38]) is given by

$$\frac{\partial}{\partial x} \frac{\partial \phi}{\partial t} = \dot{U} - U \frac{\partial^2 \phi}{\partial x^2} \tag{15}$$

In numerical calculation, $\partial^2\phi/\partial x^2$ can be evaluated by

$$-\left(\frac{\partial^2\phi}{\partial z^2}+\frac{\partial^2\phi}{\partial y^2}\right)$$

through the values of the potential on the wave maker.

3. FINITE ELEMENT FORMULATION AND NUMERICAL PROCEDURE

At each time step, a mixed boundary value problem has to be solved in which the unknown functions satisfy the Laplace equation in the fluid domain, the Dirichlet condition on the free surface and on the far end, and the Neumann condition on the rigid surface. The FEM is used in which the fluid domain is discretized into a set of small elements and the velocity potential is expressed in terms of a shape function, $N_J(x, y, z)$

$$\phi = \sum_J \phi_J N_J(x, y, z) \tag{16}$$

where ϕ_J is the velocity potential at the nodes. The shape function may be taken as a linear, quadratic or higher-order polynomial function. In this work, linear shape functions are used because this choice makes the calculation of influence coefficients relatively simple. Using the Galerkin method, the Laplace equation and the boundary conditions satisfied by the velocity potential can be discretized in the following form [39,40]:

$$\iiint_\forall \nabla N_I \cdot \sum_{\substack{J \\ J\notin S_p}} \phi_J \nabla N_J \, \mathrm{d}\forall = \iint_{S_\mathrm{n}} N_I f_\mathrm{n} \, \mathrm{d}S - \iiint_\forall \nabla N_I \cdot \sum_{\substack{J \\ J\in S_p}} (f_p)_J \nabla N_J \, \mathrm{d}\forall \quad (I\notin S_p) \tag{17}$$

where S_p represents the Dirichlet boundary on which the velocity potential, denoted by f_p, is known and S_n represents the Neumann boundary on which the normal derivative of the velocity potential, denoted by f_n, is known. Equation (17) can further be written in the matrix form

$$[A]\{\phi\} = \{B\} \tag{18}$$

where

$$\{\phi\} = [\phi_1, \phi_2, \phi_3, \ldots, \phi_I, \ldots]' \quad (I\notin S_p) \tag{19}$$

$$A_{IJ} = \iiint_\forall \nabla N_I \cdot \nabla N_J \, \mathrm{d}\forall \quad (I\notin S_p \text{ and } J\notin S_p) \tag{20}$$

$$B_I = \iint_{S_\mathrm{n}} N_I f_\mathrm{n} \, \mathrm{d}S - \iiint_\forall \nabla N_I \sum_{\substack{J \\ J\in S_p}} (f_p)_J \nabla N_J \, \mathrm{d}\forall \quad (I\notin S_p) \tag{21}$$

It should be noted that the terms associated with the velocity potential on the free surface appear on the right-hand side of Equation (17) or (18). They are known, i.e. $\phi_J = (f_p)_J$, when solving the equation.

3.1. Discretization of the fluid domain

The discretization of the fluid domain into a mesh of small elements is a fundamental part of the numerical procedure. There is considerable literature on this topic (see, for example, Reference [41]). The work presented here is primarily directed towards wave interactions with vertical cylinders. This allows some relatively simple techniques to be used. The fluid domain is first divided into a number of small hexahedra by three groups of surfaces. One group consists of curved surfaces (referred to as horizontal surfaces) roughly lying in horizontal directions. The other two groups of surfaces are in the transverse and longitudinal directions of the tank, respectively. The hexahedra generated in this way are then divided into six tetrahedra, as shown in Figure 2. The tetrahedra constitute the elements required.

The distance between the surfaces may change in order to achieve a relatively finer discretization in the regions where the fluid velocity is expected to be larger, which may improve the accuracy without increasing the CPU time. Wu and Eatock Taylor [17,18] suggested that the distance between the horizontal surfaces near the free surface should be smaller than well below the surface, and determined by

$$z_j = \frac{\exp[-\kappa(d+\zeta)] - \exp\left[-\kappa(d+\zeta)\dfrac{j}{N}\right]}{1-\exp[-\kappa(d+\zeta)]}(d+\zeta)+\zeta \tag{22}$$

where z_j is the vertical co-ordinate of a node, N is the total number of divisions in the vertical direction and κ (≥ 0) is a coefficient that can be used to adjust the distribution of the nodes. A larger value of κ means a finer mesh near the free surface. When $\kappa = 0$, the mesh is uniform in the vertical direction. Physically, the amplitude of the fluid velocity in waves decays with water depth, the rate of the decay depending on the ratio of the wavelength to the water depth: the smaller the ratio, the faster the decay. Thus, a larger value of κ should be used for smaller wavelength/depth ratios, which leads to smaller elements near the free surface and larger ones

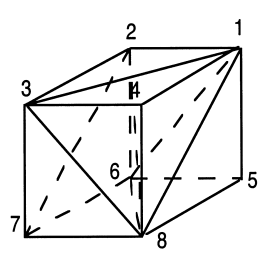

Figure 2. Division of a hexahedron.

near the bottom. However, when the coefficient is chosen, care should be taken to avoid elements with very large aspect ratios. If the ratio is too large, the resulting coefficient matrix, $[A]$, may become ill conditioned. Considering all the factors, the coefficient used in this work is

$$\kappa = -0.31\frac{d}{g}\omega^2 + 2.29\sqrt{\frac{d}{g}}\omega - 1.47 \tag{23}$$

for the frequency range discussed in Section 4, subject to

$$\kappa < \min(\kappa_1, \kappa_2) \tag{24}$$

where κ_1 and κ_2 are determined by

$$\frac{\exp\left[\dfrac{\kappa_1(d+\zeta)}{N}\right]-1}{\exp[\kappa_1(d+\zeta)]-1} = \frac{h_{xy}}{10(d+\zeta)} \tag{25a}$$

$$\frac{\exp\left[\dfrac{-\kappa_2(d+\zeta)}{N}\right]-1}{\exp[-\kappa_2(d+\zeta)]-1} = \frac{10h_{xy}}{(d+\zeta)} \tag{25b}$$

h_{xy} in the above equations represents the length of element in the horizontal direction.

3.2. Velocity calculation

The velocity field can be obtained through a mixed element method, in which both the velocity and potential are treated as unknowns and solved together. Alternatively, the velocity can be calculated using a formulation based on the Galerkin method after the potential has been found. Both techniques were used by Wu and Eatock Taylor [17] and were found to give satisfactory results. In many cases, however, only the velocity on the free surface and body surface is required. Wu and Eatock Taylor [18], therefore, suggested that the velocity on these surfaces could be calculated by a finite difference method once the potential was available. The results from some test cases showed that the latter technique could achieve similar accuracy and require far less CPU time than the other methods. This technique is adopted here, with some modifications as outlined below.

We consider the velocity on the free surface first. Figure 3 shows a typical node I on the free surface based on the mesh structure discussed in the previous section. The node is connected to four nodes, $I+1$, $I+2$, $I+3$ and $I+4$, on the free surface. A vertical line starting from node I will pass through nodes $I+5$ and $I+6$ at spacing h_1 and h_2, as shown in the figure. The vertical velocity is then evaluated using the potentials ϕ_I, ϕ_{I+5} and ϕ_{I+6} at the three nodes on the vertical line by the following equation:

$$w = \frac{2}{3h_1}\left(\frac{2h_1 + h_2}{h_1 + h_2} + \frac{1}{2}\right)\phi_I - \left(\frac{2}{3h_2} + \frac{1}{h_1}\right)\phi_{I+5} + \frac{2}{3h_1}\left(\frac{h_1}{h_1 + h_2}\right)\phi_{I+6} \tag{26}$$

This is based on the combination of a two-point (weighted by 1/3) and a three-point (weighted by 2/3) numerical differentiation formula, which is found to give more accurate results than that used by Wu and Eatock Taylor [18] for the cases considered in this work.

The horizontal components are found by grouping vectors on the free surface with two vectors in each group. The four vectors shown in Figure 3 may be divided into four groups: $(\boldsymbol{l}^1, \boldsymbol{l}^2)$, $(\boldsymbol{l}^2, \boldsymbol{l}^3)$, $(\boldsymbol{l}^3, \boldsymbol{l}^4)$ and $(\boldsymbol{l}^4, \boldsymbol{l}^1)$. For each group, the following equations can be obtained:

$$u_i l_x^k + v_i l_y^k = \frac{\partial \phi}{\partial \boldsymbol{l}^k} - w l_z^k \tag{27}$$

$$u_i l_x^m + v_i l_y^m = \frac{\partial \phi}{\partial \boldsymbol{l}^m} - w l_z^m \tag{28}$$

where l_x^k, l_y^k and l_z^k are the components of the vector $\boldsymbol{l}^k$ $(k = 1, 2, \ldots)$ in the x-, y- and z-directions. $\partial\phi/\partial\boldsymbol{l}$ in Equations (27) and (28) is evaluated by two-point differencing. The solution of Equations (27) and (28) gives u_i and v_i related to $\boldsymbol{l}^k$ and $\boldsymbol{l}^m$. The averages of u_i and v_i are taken as the horizontal velocities at the node I, using

$$u = \frac{1}{q}\sum_{i=1}^{q} u_i \tag{29}$$

$$v = \frac{1}{q}\sum_{i=1}^{q} v_i \tag{30}$$

where q is the number of groups.

On rigid surfaces such as the body surface, the normal velocity is known and only the tangential components need to be determined. In this case, the nodes I, $I+1$, $I+2$, $I+3$ and

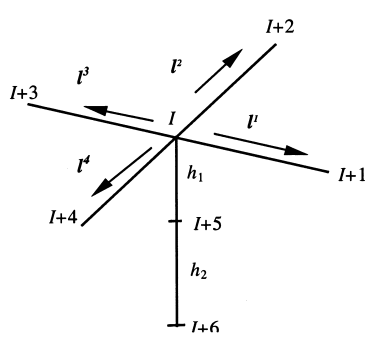

Figure 3. Node and its neighbours.

$I+4$ are taken on the body surface, and the other two nodes $I+5$ and $I+6$ in the normal direction are not needed. In order to find the two tangential components of the velocity, Equations (27) and (28) are again used with the second term on the right-hand side (the normal component) taken from boundary condition, while Equations (29) and (30) remain the same although the meanings of u and v are different.

It should be noted that the above method has been developed in the context of the meshes used in Part 2 [22] for modelling wave interaction with vertical cylinders. Modification would clearly be needed for more general applications.

3.3. Time marching on the free surface

Using the velocity, we can calculate the wave elevation and the potential on the free surface, based on Equations (2) and (3). These up-dated values provide conditions on the new boundaries for the solution at the next time step.

The free surface boundary conditions, however, only give the time derivatives of the parameters. Numerical integration must be performed to obtain the new values of the potential and free surface position. The method used here to achieve this is based on the open trapezoidal rule [42]. Suppose that the time derivative of a function y is known, i.e.

$$\left.\frac{\mathrm{d}y}{\mathrm{d}t}\right|_t = f$$

at time t. The value of the function at the next time step is determined from

$$y_{t+\Delta t} = y_t + \frac{\Delta t}{2}(3f_t - f_{t-\Delta t}) \tag{31}$$

where Δt is the time step, which is assumed to be constant. The accuracy of the equation is of the order of $(\Delta t)^2$. This formula is quite straightforward to use when the node is followed during the calculation. But this may lead to a seriously distorted mesh, especially in steep waves. Thus, remeshing has to be applied to avoid this. When this is done, evaluation of the time derivative $f_{t-\Delta t}$ at the previous step becomes problematical. The reason is that after remeshing, node J at t and node J at $t-\Delta t$ may not represent the same fluid particle. The information about node J at $t-\Delta t$ has to be interpolated from the nodes where the corresponding information is available. More details about this can be found in Ma [43].

3.4. Remeshing and interpolation

If the nodes are followed throughout the calculation, the configuration of elements will change during the time marching process. It is possible that the elements may become so distorted that the calculation breaks down. To overcome this problem, remeshing may be used at each time step or after every several time steps. The remeshing methodology is the same as that described in Section 3.1. Figure 4 shows the procedure for the remeshing on the free surface. Triangle abc is a part of the free surface at time $t-\Delta t$. After the solution has been found, the nodes a, b and c are updated to a', b' and c', respectively. Consequently, the triangle changes to

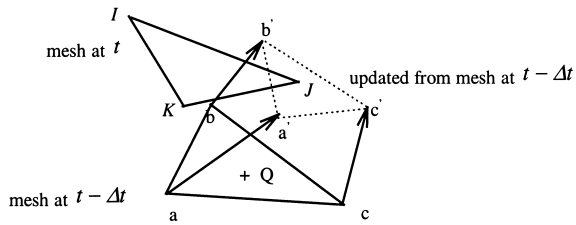

Figure 4. Illustration of remeshing.

$a'b'c'$. If remeshing is performed at this time level, new triangles on the free surface are formed (triangle IJK in the figure denotes one of them). The new nodes (I, J, K, . . .) may not necessarily coincide with the old nodes (a', b', c', . . .). All the information is held at the nodes a', b' and c', but the values at the nodes I, J and K are needed for calculation at time t. In order to find the values at the new nodes, a straightforward interpolation may be employed. One must, however, find which old triangle each new node, such as J, belongs to before performing the interpolation because when the fluid domain is remeshed, the new node may not automatically be attached to a particular old triangle. To find the corresponding old triangle, the following method is used.

Consider node J specifically. For convenience, triangle $a'b'c'$ is projected on to the oxy plane to form $a''b''c''$, as shown in Figure 5. Then, the following six vectors can be defined:

$$\boldsymbol{VJ}_1 = \{x_J - x_{a''}, y_J - y_{a''}\}$$

$$\boldsymbol{VJ}_2 = \{x_J - x_{b''}, y_J - y_{b''}\}$$

$$\boldsymbol{VJ}_3 = \{x_J - x_{c''}, y_J - y_{c''}\}$$

$$\boldsymbol{V}_{ba} = \{x_{b''} - x_{a''}, y_{b''} - y_{a''}\}$$

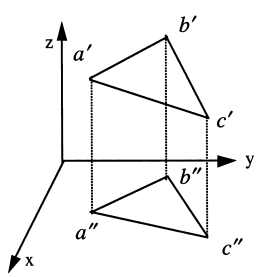

Figure 5. Projection of triangle $a'b'c'$ onto the x–y plane.

$$\boldsymbol{V}_{cb} = \{x_{c''} - x_{b''}, y_c - y_{b''}\}$$

$$\boldsymbol{V}_{ac} = \{x_{a''} - x_{c''}, y_{a''} - y_{c''}\}$$

where x, y and z are the co-ordinates of corresponding points denoted by the subscripts. If the node J is inside the triangle $a'b'c'$, it must follow that

$$\begin{cases} \boldsymbol{VJ}_1 \times \boldsymbol{V}_{ba} \geq 0 \\ \boldsymbol{VJ}_2 \times \boldsymbol{V}_{cb} \geq 0 \\ \boldsymbol{VJ}_3 \times \boldsymbol{V}_{ac} \geq 0 \end{cases} \tag{32}$$

If one of inequalities (32) is not satisfied, node J must be outside the triangle. The search will move to the next triangle until all conditions (32) are satisfied.

Numerical evidence has suggested that if the remeshing is carried out too frequently, remeshing after every time step, for example, the interpolation used above may cause a loss of energy. Interpolation based on a quadratic function has also been tested, but the problem of energy loss still exists, although it may be slightly reduced. To overcome this difficulty, remeshing should be performed as little as possible. On the other hand, overdistortion may occur if remeshing is applied too infrequently. In this work, remeshing is carried out after every 20–100 steps depending on the wavelength.

3.5. Recovery techniques

Like other numerical methods, the FEM can only offer an approximation to the exact solution of the problem. The difference between the exact solution and the finite element solution may be a result of modelling a continuum with a computational model that has a finite number of degrees of freedom and representing a continuous function with a piecewise interpolation function. Although the difference, or error, may decrease with an increase in the number of elements, very large numbers of elements are not always economical or practical. In solid mechanics, efforts have been made to develop a good postprocessing method and an adaptive mesh procedure (see, for example, References [44–46]). These two distinct research efforts serve the same purpose, i.e. to achieve higher accuracy without a marked increase in computational cost. Postprocessing techniques aim to provide more accurate results by properly treating the finite element solution. By contrast, the adaptive mesh method is employed to try to achieve more accurate results by optimizing the distribution of elements, so that finer meshes are used in regions of strongly variable gradient, and coarser meshes used elsewhere. This optimization procedure is performed by adjusting the mesh according to the errors obtained through successively solving the same problem. The core of the adaptive technique is the error estimation, which is based on some postprocessing of results. It can, therefore, be seen that postprocessing is fundamental to improving the quality of the finite element solution. In solid mechanics, postprocessing is mainly performed on stresses (derivatives) if the FEM is applied to displacements. Several techniques have been used to postprocess the stresses [44]. Superconvergent patch recovery is one of them, developed by Zienkiewicz and Zhu [45].

In this work, we do not attempt to use the above-mentioned form of mesh adaptation. Instead, we improve the finite element results by using a patch recovery technique. The fundamental idea behind this technique is that the velocity is assumed to be fitted by a polynomial over a patch on the free surface. Such a patch consists of a union of triangles containing a particular node, as shown in Figure 6, where there are six triangles in the patch associated with node I. The polynomial can be written simply as

$$w_I^* = a + bx + cy \tag{33}$$

where w_I^* denotes a fitted velocity component on the free surface, and the subscript refers to the patch around the node I. The coefficients a, b and c in Equation (33) are determined by a least-squares method through fitting the equation to a set of sampling points. Thus, the following function is minimized:

$$\Lambda = \sum_{i=1}^{m} (a + bx_i + cy_i - w_i^h)^2 \tag{34}$$

where x_i and y_i are the horizontal co-ordinates of the sampling points, w_i^h is the velocity component at the point, and m is the number of triangles in this patch. The minimization of Equation (34) leads to

$$\begin{bmatrix} 1 & \sum_{i=1}^{m} x_i & \sum_{i=1}^{m} y_i \\ \sum_{i=1}^{m} x_i & \sum_{i=1}^{m} x_i^2 & \sum_{i=1}^{m} x_i y_i \\ \sum_{i=1}^{m} y_i & \sum_{i=1}^{m} x_i y_i & \sum_{i=1}^{m} y_i^2 \end{bmatrix} \begin{Bmatrix} a \\ b \\ c \end{Bmatrix} = \begin{Bmatrix} \sum_{i=1}^{m} w_i^h \\ \sum_{i=1}^{m} x_i w_i^h \\ \sum_{i=1}^{m} y_i w_i^h \end{Bmatrix}$$

Once the solution of a, b and c is found from this equation, Equation (33) enables the new velocity $\bar{w}_I$ to be evaluated at node I. We refer to $\bar{w}_I$ as the recovered velocity and it is used to replace the corresponding velocity calculated in Section 3.2. Clearly, the velocities at the sampling points w_i^h determine the new velocity found in this way. If the w_i^h have higher

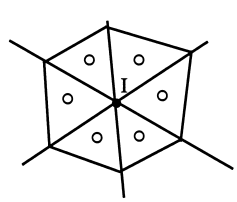

Figure 6. Triangular patch (○, sampling point).

accuracy (i.e. are better approximations to the exact velocities), $\bar{w}_I$ may be more accurate than those calculated in Section 3.2. In this case, the sampling points are called *superconvergent* points. Zienkiewicz and Zhu [45] showed that when using triangular elements with a linear interpolation function in the finite element analysis, the centroid of the element is a superconvergent point, where the numerical solution is more accurate than at other points. Therefore, we take the sampling points as being the centroids of the triangles and estimate w_i^h using the element shape function.

A difficulty in using the recovery technique may occur, however, at the intersection of the free surface and a solid boundary, where a patch may include fewer triangles, as shown in Figure 7. Although various techniques have been suggested to deal with this problem, none is perfect. One of them is given by Zienkiewicz and Zhu [45], in which the values of stresses on the boundary are obtained using the patches of internal nodes, somewhat like extrapolation.

In our work, different treatments are used for different boundary edges. If the edges are composed of straight lines, such as (a) and (b) in Figure 7, a five-point smoothing technique similar to that used by Longuet-Higgins and Cokelet [1] is applied. If the edge is a curve like case (c) in Figure 7, we simply follow the idea of Zienkiewicz and Zhu [45], based on extrapolation. That is, the value at point A in Figure 7(c) is found using the patch associated with internal point B.

3.6. Solution of the algebraic equations

The solution of the algebraic system in Equation (18) is a key part of the analysis discussed in this paper. The efficiency of the corresponding code largely depends on the efficiency of the solution technique used. There is a number of possible methods for solving the system but the efficiency of each method is largely problem-dependent. A considerable number of tests have been performed in this work to investigate the efficiency of three methods. One is the direct method based on Choleski factorization with optimization of the numbering system of the nodes. The two other methods are based on the conjugate gradient iterative procedure with different preconditioners: (1) symmetric successive overrelaxation (SSOR) and (2) incomplete Choleski factorization (ILU). Both preconditioners include an artificial parameter to adjust their performance. These three methods have been used to solve several problems. It has been found that the iterative method with the SSOR preconditioner is generally the most efficient among the three methods. An artificial parameter to adjust the performance of the preconditioner has been carefully chosen. Further details can be found in Ma [43].

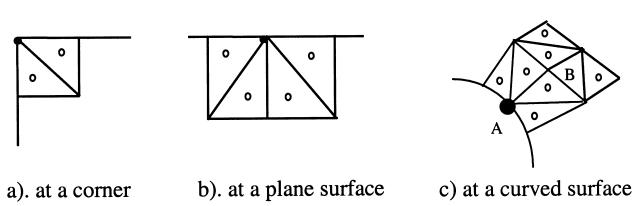

Figure 7. Patch around the boundary nodes.

4. CONCLUSION

In this paper, a methodology and the corresponding numerical algorithm have been described to simulate the three-dimensional interaction between fixed bodies and waves. It uses a time marching procedure based on fully non-linear potential theory. The main feature is that the boundary value problem at each time step is solved by an FEM. The recovery technique has been implemented to improve the FEM solution. A radiation condition based on the combination of damping zone and Sommerfeld condition is employed. The corresponding algebraic equations have been solved using a conjugate gradient iterative method with an SSOR preconditioner. The work is primarily aimed at wave interactions with vertical cylinders. Many of the techniques described here, such as the methods of mesh generation and velocity calculation, have been tailored mainly to this kind of configuration. They could be readily extended to more general cases. Numerical results and validation are reported in Part 2 of this study [22].

ACKNOWLEDGMENTS

This work was sponsored by research grant GR/K80372 from the UK Engineering and Physical Sciences Research Council.

REFERENCES

1. Longuet-Higgins MS, Cokelet ED. The deformation of steep surface waves on water: I. A numerical method of computation. *Proceedings of the Royal Society of London A* 1976; **350**: 1–26.
2. Isaacson M, Cheung KF. Second order wave diffraction around two-dimensional bodies by time domain method. *Applied Ocean Research* 1991; **13**: 175–186.
3. Isaacson M, Ng JYT. Time-domain second-order wave radiation in two dimensions. *Journal of Ship Research* 1993; **37**: 25–33.
4. Zhang S, Williams AN. Time-domain simulation of the generation and propagation of second-order Stokes waves in a two-dimensional wave flume. Part I: monochromatic wavemaker motions. *Journal of Fluids and Structures* 1996; **10**: 319–335.
5. Skourup J, Büchmann B, Bingham H. A second order 3D BEM for wave-structure interaction. In *12th International Workshop on Water Waves and Floating Bodies*, Carry-le-Rouet, France, Molin B (ed.), 1997.
6. Faltinsen OM. Numerical solution of transient nonlinear free surface motion outside or inside moving bodies. In *Proceedings of the 2nd International Conference on Numerical Ship Hydrodynamics*, Berkeley, CA, Schot JW, Salvesen N (eds), 1977; 347–357.
7. Vinje T, Brevig P. Nonlinear ship motions. In *Proceedings of the 3rd International Conference on Numerical Ship Hydrodynamics*, Paris, France, Dern JC, Haussling HJ (eds), 1981; 257–268.
8. Lin WM, Newman JN, Yue DK. Nonlinear forced motion of floating bodies. In *Proceedings of the 15th Symposium on Naval Hydrodynamics*, Hamburg, Germany. National Academy Press: Georgetown, SC, 1984; 33–49.
9. Kang C-G, Gong I-Y. A numerical solution method for three-dimensional nonlinear free surface problems. In *Proceedings of the 18th Symposium on Naval Hydrodynamics*, Ann, Arbor, MI. National Academy Press: Georgetown, SC, 1990; 427–430.
10. Chan JLK, Calisal SM. A numerical procedure for time domain nonlinear surface wave calculations. *Ocean Engineering* 1993; **20**: 19–32.
11. Ferrant P. Radiation and diffraction of nonlinear waves in three dimensions. In *Proceedings of the International Conference on Behaviour of Offshore Structures*, MIT, USA, Chryssostonidis C (ed.). Redwood Books: Trowbridge, 1994; 507–524.
12. Celebi MS, Kim MH. Nonlinear wave-body interactions in a numerical wave tank. In *12th International Workshop on Water Waves and Floating Bodies*, Carry-le-Rouet, France, Molin B (ed.), 1997.

13. Celebi MS, Kim MH, Beck RF. Fully nonlinear 3D numerical wave tank simulation. *Journal of Ship Research* 1998; **42**: 33–45.
14. Cao Y, Schultz WW, Beck RF. Three-dimensional desingularised boundary integral method for potential problems. *International Journal for Numerical Methods in Fluids* 1991; **12**: 785–803.
15. Beck RF, Cao Y, Scorpio S, Schultz WW. Nonlinear ship motion computations using the desingularised method. In *Proceedings of the 20th Symposium on Naval Hydrodynamics*, U.C., Santa Barbara, CA. National Academy Press: Georgetown, SC, 1994.
16. Wang P, Yao Y, Tulin M. An efficient numerical tank for nonlinear water waves, based on the multi-subdomain approach with BEM. *International Journal for Numerical Methods in Fluids* 1995; **20**: 1315–1336.
17. Wu GX, Eatock Taylor R. Finite element analysis of two dimensional non-linear transient water waves. *Applied Ocean Research* 1994; **16**: 363–372.
18. Wu GX, Eatock Taylor R. Time stepping solutions of the two dimensional non-linear wave radiation problem. *Ocean Engineering* 1995; **22**: 785–798.
19. Cai X, Langtangen HP, Nielsen BF, Tveito A. A finite element method for fully nonlinear water waves. *Journal of Computational Physics* 1998; **143**: 544–568.
20. Westhuis JH, Andonowati AJ. Applying the finite element method in numerically solving the two dimensional free-surface water wave equations. In *13th International Workshop on Water Waves and Floating Bodies*, Alphen aan den Rijn, The Netherlands, Hermans AJ (ed.), 1998; 171–174.
21. Ma QW, Wu GX, Eatock Taylor R. Finite element analysis of the non-linear transient waves in a three dimensional long tank. In *12th International Workshop on Water Waves and Floating Bodies*, Carry-le-Rouet, France, Molin B (ed.), 1997.
22. Ma QW, Wu GX, Eatock Taylor R. Finite element simulation of fully nonlinear interaction between vertical cylinders and steep waves. Part 2. Numerical results and validation. *International Journal for Numerical Methods in Fluids* 2001; **36**: 287–308.
23. Chan RK-C. Finite difference simulation of the planar motion of a ship. In *Proceedings of the 2nd International Conference on Numerical Ship Hydrodynamics*, Berkeley, CA, Schot JW, Salvesen N (eds), 1977; 39–56.
24. Broeze J, Romate JE. Absorbing boundary condition for free surface wave simulations with a panel method. *Journal of Computational Physics* 1992; **99**: 146–158.
25. Maisondieu C, Clement A. A realisable force feedback–feedforward control loop for a piston wave absorber. In *8th International Workshop on Water Waves and Floating Bodies*, St. John's, Newfoundland, Pawlowski J (ed.), 1993.
26. Skourup J, Schaffer HA. Wave generation and active absorption in a numerical wave flume. In *Proceedings of the International Symposium on Offshore and Polar Engineering Conference*, Hawaii, vol. 3, Dos Santos JF, Langen I, Ellinas CP (eds), 1997; 85–91.
27. Cointe R, Geyer P, King B, Molin B, Tramoni M. Nonlinear and linear motions of a rectangular barge in a perfect fluid. In *Proceedings of the 18th Symposium on Naval Hydrodynamics*, *University of Michigan*, Ann Arbor, MI, 1990; 85–98.
28. Arai M, Paul UK, Cheng LY, Inoue Y. A technique for open boundary treatment in numerical wave tanks. *Journal of the Society of Naval Architecture of Japan* 1993; **173**: 45–50.
29. Contento G, Casole S. On the generation and propagation of waves in 2D numerical wave tanks. *ISOPE '95*. Netherlands, 1995; **3**: 10–18.
30. Clement A. Coupling of two absorbing boundary conditions for 2D time-domain simulations of free surface gravity waves. *Journal of Computational Physics* 1996; **126**: 139–151.
31. Orlanski I. A simple boundary condition for unbounded hyperbolic flows. *Journal of Computational Physics* 1976; **21**: 251–269.
32. Zhou Z, Gu M. A numerical research on nonlinear body-wave interaction. In *Proceedings of the 18th Symposium on Naval Hydrodynamics*, Ann Arbor, MI, 1990; 103–117.
33. Ohyama T. Development of a numerical wave tank for analysis of non-linear and irregular wave fields. *Fluid Dynamics Research* 1991; **8**: 231–251.
34. Lee JF, Leonard JW. A time-dependent radiation condition for transient wave-structure interactions. *Ocean Engineering* 1987; **14**: 469–488.
35. Cao Y, Beck RF, Schultz W. An absorbing beach for numerical simulation of non-linear waves in a wave tank. In *8th International Workshop on Water Waves and Floating Bodies*, St. John's, Newfoundland, Pawlowski J (ed.), 1993.
36. Eatock Taylor R, Wang BT, Wu GX. On the transient analysis of the wavemaker. In *9th International Workshop on Water Waves and Floating Bodies*, Kuju, Oita, Japan, Ohkusu M (ed.), 1994.
37. Crapper GD. *Introduction to Water Waves*. Ellis Horwood: Chichester, 1984.

38. Wu GX. Hydrodynamic force on a rigid body during impact with liquid. *Journal of Fluids and Structures* 1998; **12**: 549–559.
39. Wu GX, Ma QW, Eatock Taylor R. Analysis of interaction between nonlinear waves and bodies by domain decomposition. In *Proceedings of the 21st Symposium on Naval Hydrodynamics*, Trondheim, Norway. National Academy Press: Georgetown, SC, 1996; 110–119.
40. Wu GX, Ma QW, Eatock Taylor R. Numerical simulation of sloshing waves in a 3D tank based on a finite element method. *Applied Ocean Research* 1998; **20**: 337–355.
41. Greaves DM. *Numerical modelling of laminar separated flows and inviscid steep waves using adaptive hierarchical meshes*. DPhil thesis, University of Oxford, 1995.
42. Korn GA, Korn TM. *Mathematical Handbook for Scientists and Engineers*. McGraw-Hill: New York, 1968.
43. Ma QW. *Numerical simulation of nonlinear interaction between structures and steep waves*. PhD thesis, Department of Mechanical Engineering, University College London, UK, 1998.
44. Zienkiewicz OC, Taylor RL. *The Finite Element Method*, vols. 1 and 2. McGraw-Hill: New York, 1994.
45. Zienkiewicz OC, Zhu JZ. The superconvergent patch recovery and a posterior error estimators. Part 1. The recovery technique. *International Journal for Numerical Methods in Engineering* 1992; **33**: 1331–1364.
46. Wiberg NE, Abdulwahab F, Ziukas S. Enhanced superconvergent patch recovery incorporating equilibrium and boundary conditions. *International Journal of Numerical Methods in Engineering* 1994; **37**: 3417–3440.

